FEBS Letters

FEBS PRESS science publishing by scientists

Ile209 of *Leishmania donovani* xanthine phosphoribosyltransferase plays a key role in determining its purine base specificity

Bhumi Patel[1], Dhaval Patel[1] and Anju Pappachan[1,2]

1 Indian Institute of Advanced Research (Puri Foundation for Education in India), Koba Institutional Area, Gandhinagar, India
2 School of Life Sciences, Central University of Gujarat, Gandhinagar, India

Correspondence
A. Pappachan, School of Life Sciences, Central University of Gujarat, Sector 30, Gandhinagar 382030, Gujarat, India
Tel: +91 79 23260416
E-mail: anjupappachan@gmail.com; anju.p@cug.ac.in

(Received 9 February 2021, revised 21 June 2021, accepted 2 July 2021, available online 26 July 2021)

doi:10.1002/1873-3468.14162

Edited by Michael Ibba

Xanthine phosphoribosyltransferase (XPRT) and hypoxanthine-guanine phosphoribosyltransferase (HGPRT) are purine salvaging enzymes of *Leishmania donovani* with distinct 6-oxopurine specificities. LdXPRT phosphoribosylates xanthine, hypoxanthine, and guanine, with preference toward xanthine, whereas LdHGPRT phosphoribosylates only hypoxanthine and guanine. In our study, LdXPRT was used as a model to understand these purine base specificities. Mutating I209 to V, the conserved residue found in HGPRTs, reduced the affinity of LdXPRT for xanthine, converting it to an HGXPRT-like enzyme. The Y208F mutation in the active site indicated that aromatic residue interactions with the purine ring are limited to pi-pi binding forces and do not impart purine base specificity. Deleting the unique motif (L55-Y82) of LdXPRT affected enzyme activity. Our studies established I209 as a key residue determining the 6-oxopurine specificity of LdXPRT.

Keywords: guanine; hypoxanthine; Leishmania; phosphoribosyltransferases; purine salvage; purine specificity; xanthine; xanthine phosphoribosyltransferase

Leishmania donovani, the protozoan parasite causing visceral leishmaniasis lacks the metabolic machinery required for the *de novo* synthesis of purine nucleotides. Hence, it salvages purine bases from the human host [1]. Due to the critical dependence of *L. donovani* on the purine salvage pathway, enzymes acting in this pathway could serve as a suitable target for antileishmanial chemotherapy [2]. *Leishmania* has three phosphoribosyl transferases that convert dephosphorylated purines to nucleosides monophosphates: hypoxanthine-guanine phosphoribosyltransferase (HGPRT), xanthine phosphoribosyltransferase (XPRT), and adenine phosphoribosyltransferase (APRT) [3]. XPRT and HGPRT are specific for 6-oxopurines. Of the two, the enzyme XPRT of *L. donovani* has been a focus of attention due to its notable absence in mammals. Our earlier studies [4] have shown that there are also significant structural differences between LdXPRT and its closest human counterpart, that is, HGPRT, therefore making it an attractive target for selective inhibition. Null mutational studies have also shown that the XPRT activity alone is sufficient to salvage adenine, hypoxanthine, and guanine in *L. donovani* promastigotes [5,6].

LdXPRT in addition to converting xanthine to xanthine monophosphate can also convert hypoxanthine to inosine monophosphate and guanine to guanine

Abbreviations
APRT, Adenine phosphoribosyltransferase; CD, Circular dichroism; GMP, Guanosine 5′-monophosphate; GPRT, guanine phosphoribosyltransferase; HGXPRT, hypoxanthine-guanine-xanthine phosphoribosyltransferase; IMP, Inosine 5′-monophosphate; LdHGPRT, *Leishmania donovani*-hypoxanthine-guanine phosphoribosyltransferase; LdXPRT, *Leishmania donovani*-Xanthine phosphoribosyltransferase; PRPP, 5-Phospho-α-D-ribose 1-diphosphate; PRT, Phosphoribosyltransferase; XMP, Xanthosine 5′-monophosphate.

monophosphate, albeit with a lesser affinity toward hypoxanthine and guanine compared to xanthine, whereas the LdHGRPT can phosphoribosylate only hypoxanthine and guanine but not xanthine. A unique XPRT gene is present only in few organisms such as *Leishmania*, certain fungi, and bacteria [4]. Xanthine phosphoribosylating enzymes in other organisms like *P. falciparum* [7], *T. gondii* [8], and *T. foetus* [9] is the hypoxanthine-guanine-xanthine PRT (HGXPRT) which prefers hypoxanthine and guanine as a substrate over xanthine. However, the LdXPRT substrate profile is different from the HGXPRT enzymes, as it favors xanthine over hypoxanthine and guanine. This unique substrate specificity of LdXPRT compared to other purine PRTs as well as its intriguing presence in *Leishmania* along with a separate HGPRT makes it an ideal model to investigate the molecular determinants of the unique purine base specificity of PRTs.

Crystal structures of purine PRTs show a conserved PRPP-binding domain and a less conserved purine-binding domain. The latter domain shows variations in amino acid residues among different purine PRTs [9] which might play a crucial role in the purine base specificity of these enzymes. There are earlier reports of alteration of the PRT substrate specificity by single amino acid substitutions [9,10]. Since the 6-oxopurines (xanthine, hypoxanthine, and guanine) differ only by the substituents on the C-2 atom of their purine ring, we hypothesized that the residues interacting specifically with these atoms may be critical in determining the purine base specificity of PRT enzymes.

Based on sequence and structure comparisons with other PRTs, especially with *Leishmania terantolae* HGPRT-GMP (PDB ID: 1PZM) structure, we identified certain residues and a domain that may be important for this specificity in LdXPRT [4]. In the present study, we investigated the amino acids interacting with the substituent on C-2 atom of purine ring (Ile 209 and Glu 215), an aromatic residue forming stacking interactions with the purine ring (Tyr 208) as well as a unique motif (Leu 55 to Tyr 82) found in leishmanial XPRTs through mutational studies. Previous reports on the mutational study of E215D showed that Glu 215 alone cannot be the determinant for purine base specificity of LdXPRT [11]. Hence in the present study, we mutated E215D together with the I209V. Based on our detailed sequence and structure analysis, we generated four mutants of LdXPRT (ldxprtY208F, ldxprtI209V, ldxprtI209V;E215D, and ldxprtL55_Y82del). Characterization of the mutant proteins through enzyme assays and biophysical methods could evince the role of these residues in governing the purine base specificity of LdXPRT.

Materials and methods

Materials

All the chemicals used in the present study were molecular biology grade. The chemicals for enzyme kinetic assays including hypoxanthine, guanine, xanthine, and PRPP were purchased from Sigma-Aldrich Corporation (St. Louis, MO, USA). High-fidelity DNA polymerase (iProof™) and other enzymes were procured from Bio-Rad (Hercules, CA, USA) and Thermo Fisher Scientific (Waltham, MA, USA), respectively.

Structural modeling and sequence comparison

The LdXPRT sequence (UniProtKB-Q9U6Y2) was retrieved from the Universal protein resource database (http://www.uniprot.org/). The LdXPRT model was generated by the homology modeling program SWISS-MODEL [12] using *T. brucei* HGXPRT (PDB ID: 6MXC) structure [13] as a template. The model was minimized using the ModRefiner program [14], and the stereo-chemical properties of the energy minimized model were evaluated by Ramachandran statistics using the program RAMPAGE [15]. The quality of the minimization model was also checked using the Verify 3DE [16] and ERRAT plot [17]. The refined LdXPRT model was superimposed over the crystal structure of the *L. tarentolae* HGPRT-GMP complex (PDB ID: 1PZM) to compare the active-site residues. The structures were superimposed using PYMOL [18]. Multiple sequence alignment of LdXPRT with other 6-oxopurine PRTs was carried out using the ClustalW program [19]. The PRT enzyme sequences were downloaded from NCBI (https://www.ncbi.nlm.nih.gov/) and UniProt (https://www.uniprot.org/) databases.

Site-directed mutagenesis

Site-directed mutations were introduced in the LdXPRT gene by polymerase chain reaction using our previously generated pET 15b-LdXPRT construct, as template [4]. Primers were designed and synthesized with additional restriction sites to allow easy selection of mutants (Table S1). Restriction sites were introduced by modifying nucleotides in such a way that their amino acid codon remains the same. Primers of deletion mutant were synthesized with phosphorylated 5' end for the ligation. Following the polymerase chain reaction, mutant plasmids were transformed and amplified into *E. coli* strain DH5α and were sequenced to verify mutations.

Expression and purification of LdXPRT mutants

The mutant plasmids were transformed into the Rosetta (DE3) cells for expression. The cells were grown on LB agar media supplemented with ampicillin (50 $\mu g \cdot mL^{-1}$) and

chloramphenicol (34 μg·mL^{-1}), and the expression was induced by adding 0.1 mM IPTG at 18 °C for 16 h. The cells were harvested by centrifugation at 8000 ***g*** at 4 °C for 10 min and were suspended in the lysis buffer containing 50 mM Tris/HCl, pH 7, 10 mM $MgCl_2$, 200 mM NaCl, 10% glycerol, 0.1% Triton X-100, and 1 mM PMSF. The cells were lysed in a sonicator followed by centrifugation at 12 000 ***g*** for 20 min at 4 °C, and the lysate was loaded on a HIS-Select HF Nickel Affinity Gel column, pre-equilibrated with equilibration buffer (50 Tris/HCl buffer, pH 7, 10 mM $MgCl_2$, and 200 mM NaCl). The protein was eluted by 300 mM Imidazole and was analyzed on SDS/PAGE as per the method of Laemmli [20], and the concentration of purified proteins was determined by the Bradford method. The purified proteins were dialyzed in 50 mM Tris/HCl buffer, pH 7, 10 mM $MgCl_2$, and 200 mM NaCl.

Spectral analysis

The CD spectral measurements were performed on JASCO-J815 spectropolarimeter at 20 °C. The mutant proteins were dialyzed in the buffer containing 20 mM sodium phosphate, pH 6.5, and 10 mM $MgCl_2$. The far-UV CD spectra were collected at 190 to 250 nm using a 0.5 mm path length cuvette at 0.3 mg·mL^{-1} of protein concentration, and the near-UV CD spectra were collected at 250–350 nm using a 2 mm path length cuvette at 1.3 mg·mL^{-1} of protein concentration. To record the spectra of mutant proteins in the presence of ligands (XMP, GMP, and IMP), the proteins were incubated for 2 h with 500 μM of each ligand prior to the CD experiment. Data were calculated by subtracting the spectra of ligands and medium from the corresponding spectra of proteins. UV absorbance spectra were recorded on Eppendorf BioSpectrometer kinetic from 240 to 330 nm using a protein concentration of 0.8 mg·mL^{-1} protein in 50 mM sodium phosphate buffer, pH 6.5, and 10 mM $MgCl_2$.

Fluorescence quenching analysis

Fluorescence measurements were carried out on a Cary Eclipse fluorescence spectrophotometer-G9800A with a slit width of 5 nm for both the monochromators and scan speed of 600 nm·min^{-1}. Mutant proteins were diluted up to 3.9 μM in the buffer containing 50 mM Tris/HCl, pH 7, 200 mM NaCl, and 10 mM $MgCl_2$. The proteins were titrated by adding 10-12 aliquots of ligands (XMP, GMP, and IMP) from 1 mM stocks, and the samples were excited at 280 nm. The emission spectra were recorded at 27 °C, from 285 to 370 or 450 nm depending on the protein. Each titration experiment was performed in triplicates. The effective concentrations of ligands were corrected to compensate dilution effect upon the addition of each aliquot of ligand. The dissociation constant (Kd) was calculated according to the method described in reference [4].

Steady-state kinetic analysis of LdXPRT mutants

Kinetic parameters of LdXPRT mutants for nucleobase substrates xanthine, hypoxanthine, and guanine were determined by measuring the formation of their respective products, XMP at 250 nm (Δε 3900 M^{-1} cm^{-1}), IMP at 243 nm (Δε 2200 M^{-1} cm^{-1}), and GMP at 257 nm (Δε 4200 M^{-1} cm^{-1}), respectively. The assay was performed in 100 mM Tris/HCl buffer, pH 7, and 10 mM $MgCl_2$ using 1.0 cm path length on Eppendorf BioSpectrometer® kinetic equipped with a kinetic software package. Kinetic parameters were calculated by using the software GraphPad prism (San Diego, CA, USA). The K_m and k_{cat} values for nucleobase substrates were determined at 1.0 mM PRPP and either 10–250 μM xanthine, 10–250 μM guanine, or 10–1000 μM hypoxanthine. The K_m and k_{cat} values of PRPP were determined at 1.0 mM xanthine or hypoxanthine by ranging the PRPP concentrations between 10 and 1000 μM, respectively.

Results

Structural modeling and sequence comparison

The LdXPRT model was constructed using *T. brucei* HGXPRT crystal structure (PDB ID: 6MXB) as a template [13]. The LdXPRT model superposed over the *T. brucei* HGXPRT crystal structure with an RMSD of 0.394 Å. The model so generated was subjected to energy minimization for improving the overall model quality. The energy minimized model showed acceptable Ramachandran plot statistics with 100% residues in the allowed region and acceptable ERRAT plot and Verify 3D scores (Table S2). The model was superimposed over LtHGPRT-GMP (PDB ID: 1PZM) structure to compare the active sites. The active site of LtHGPRT-GMP structure shows three interactions with the guanine ring. The first interaction was between Lys 157 and 6-oxo group, and N7 atoms of the guanine ring (Fig. 1). This lysine residue (Lys 186) was conserved in LdXPRT (Fig. 2) and probably involved in binding to the 6-oxo group of xanthine. The second interaction was an aromatic stacking interaction between Phe 178 and the guanine ring. The third interaction in LdHGPRT-GMP was between Val 179 and the 2-amino, 6-oxo, and N1 group of guanine ring. The fourth interaction was between Asp 185 and the 2-amino group of guanine ring. Structural comparisons with other HGPRTs with bound substrates showed that these interacting residues and these interactions were mostly conserved across the HGPRT family. LdXPRT has a Tyr (Tyr 208) corresponding to Phe 178, Ile (Ile 209) corresponding to Val 179, and Glu (Glu 215) corresponding to Asp 185 of

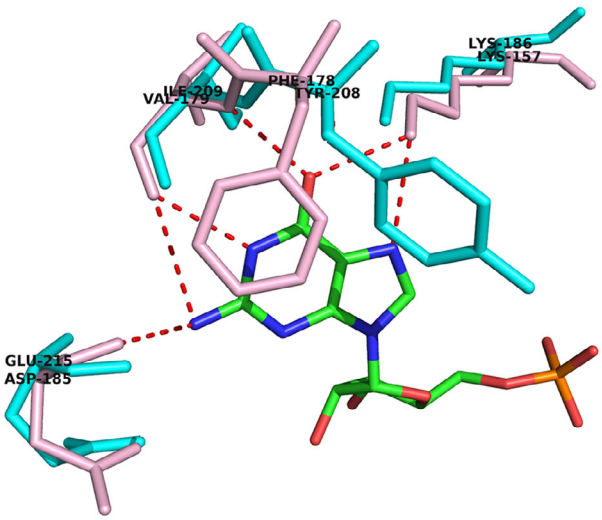

Fig. 1. Comparison of the active site of *L. tarentolae* HGPRT with LdXPRT. Residues of *L. tarentolae* HGPRT-GMP complex (PDB ID: 1PZM) are indicated by pink color. Corresponding residues in LdXPRT are indicated by cyan color.

LdHGPRT. The sequence alignment of PRTs (Fig. 2) showed that these residues (Ile 209, Glu 215, and Tyr 208) were rarely found in HGPRTs. Hence, these three amino acids were mutated to investigate their role in the substrate specificity of LdXPRT.

From our earlier studies, we had identified a 28 residue long unique motif (Leu 55 to Tyr 82) in LdXPRT which was absent in other PRT enzymes. Molecular dynamic studies indicated that this region might be having a long-range interaction with the active site [4].

Site-Directed Mutagenesis and enzyme purification

Based on *in silico* analysis, four mutants of LdXPRT were generated by polymerase chain reactions. We mutated Ile 209 to a Val, the conserved residue found in place of Ile in most HGPRTs (ldxprtI209V). Since previous reports on the mutational study of E215D in LdXPRT showed that mutating Glu 215 alone to an Asp does not alter purine base specificity of LdXPRT [11], in our study, we generated a double mutant—ldxprtI209V;E215D in which the Glu 215 was mutated to Asp and Ile 209 was mutated to Val. Tyr 208 in LdXPRT was mutated to Phe (ldxprtY208F). A deletion mutant of LdXPRT where residues from Leu 55 to Tyr 82 were deleted was generated to check the role of this motif in the enzyme activity. All the PCR amplified mutant genes were transformed and amplified into *E. coli* DH5α cells. The mutants were screened by digestion with specific restriction endonucleases and verified by sequencing. The expression of LdXPRT mutants was obtained in *E. coli* Rosetta (DE3) cells, and the proteins were purified by Ni-NTA affinity chromatography (Fig. 3).

Structural analysis of LdXPRT mutants by CD spectroscopy

The far-UV CD spectra showed that all the LdXPRT mutants were well folded (Fig. 4A). The mutants showed slight variations in the secondary structure content compared to the wild type.

The CD difference spectra generated by the subtraction of the far-UV CD spectrum of the LdXPRT from the ldxprtI209V showed an increase in the minima between 200 and 210 nm (Fig. 5A), indicating an alteration in the environment of the phenylalanine side chains [11,21]. This was further supported by the increase in UV absorbance of ldxprtI209V at ~ 250 nm (Fig. 5B) [11].

Similarly, a negative peak of ldxprtY208F and ldxprtI209V;E215D at ~ 227 nm in the CD difference spectra and an increase in the UV absorbance at ~ 280 nm indicate an alteration in the local environment of one or more tyrosine residues [11,22].

The effect of nucleotide substrates, XMP, GMP, and IMP on the secondary and tertiary structure pattern of LdXPRT mutants was determined by far and near-UV CD spectroscopy. The addition of XMP to LdXPRT and ldxprtY208F induces a negative shift in the far-UV CD spectra (Fig. 4B,C) indicating that the protein folds upon binding with XMP. The addition of XMP to ldxprtI209V, ldxprtI209V;E215D, and ldxprtL55_Y82del causes positive shift in the spectra. Further, this XMP-induced shift is higher than IMP and GMP (Fig. 4D–F) indicating that the higher structural change was required to accommodate XMP compared to IMP and GMP.

The addition of IMP to all the proteins causes increased ellipticity with no significant change in the pattern of near-UV CD spectra (Fig. S1). The addition of GMP to LdXPRT, ldxprtY208F, and ldxprtL55_Y82del gives a sharp negative peak at 257 nm; however, the binding of GMP to ldxprtI209V and ldxprtI209V;E215D showed a positive peak. Interestingly, LdXPRT, ldxprtY208F, and ldxprtL55_Y82del have Ile 209 in the purine-binding pocket; however, ldxprtI209V and ldxprtI209V;E215D have Val in place of Ile hence suggesting that the interaction of Ile 209 with the 2-amino group of guanine might cause the alteration in the environments of aromatic side chains of the protein.

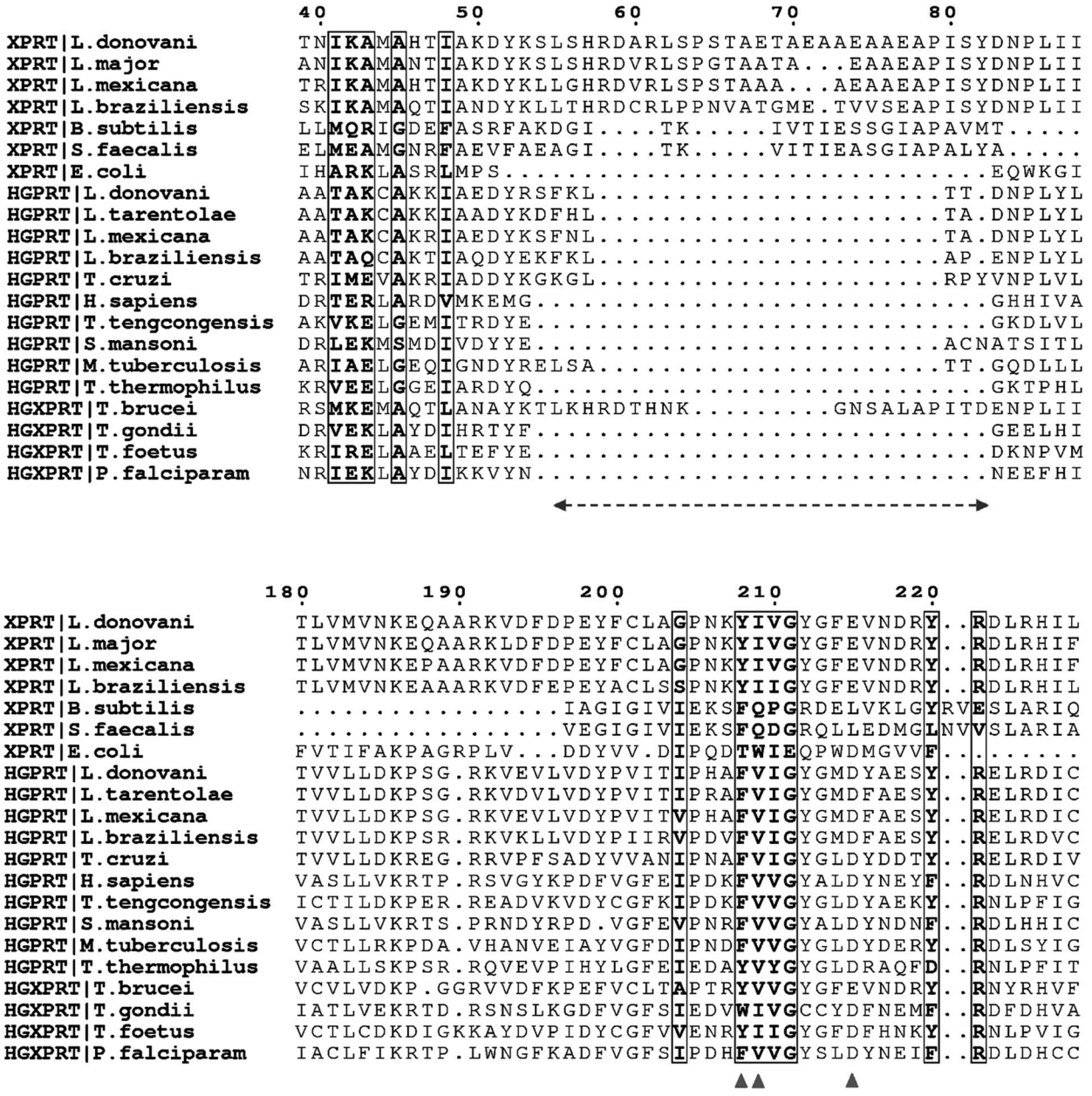

Fig. 2. Multiple sequence alignment of LdXPRT with PRT enzymes. The residues which were mutated are highlighted as (▲). The unique region (55–82) is highlighted by a dotted line.

Fluorescence spectroscopy for binding affinities of mutants with different ligands

The fluorescence emission spectra of ldxprtY208F and ldxprtI209V;E215D showed a similar emission maximum (305 nm) as wild-type protein (Fig. 6); however, λ_{max} of ldxprtI209V and ldxprtL55_Y82del shifts from 305 nm to 337 nm. Since the LdXPRT sequence does not contain tryptophan, this shift in the fluorescence spectra is likely due to the ionized form of tyrosine, that is, tyrosinate which is produced by the proton transfer to the carboxylate anion of the nearby glutamyl residues [23]. The I209V mutation might be modifying the microenvironment of the nearby glutamate residues, that is, Glu 215 to facilitate the ionization of the surrounding tyrosine (Tyr 208) to tyrosinate which gives rise to abnormal emission at around 340 nm. Similarly, the structural changes occurring due to the absence of the motif in the ldxprtL55_Y82del might be creating a

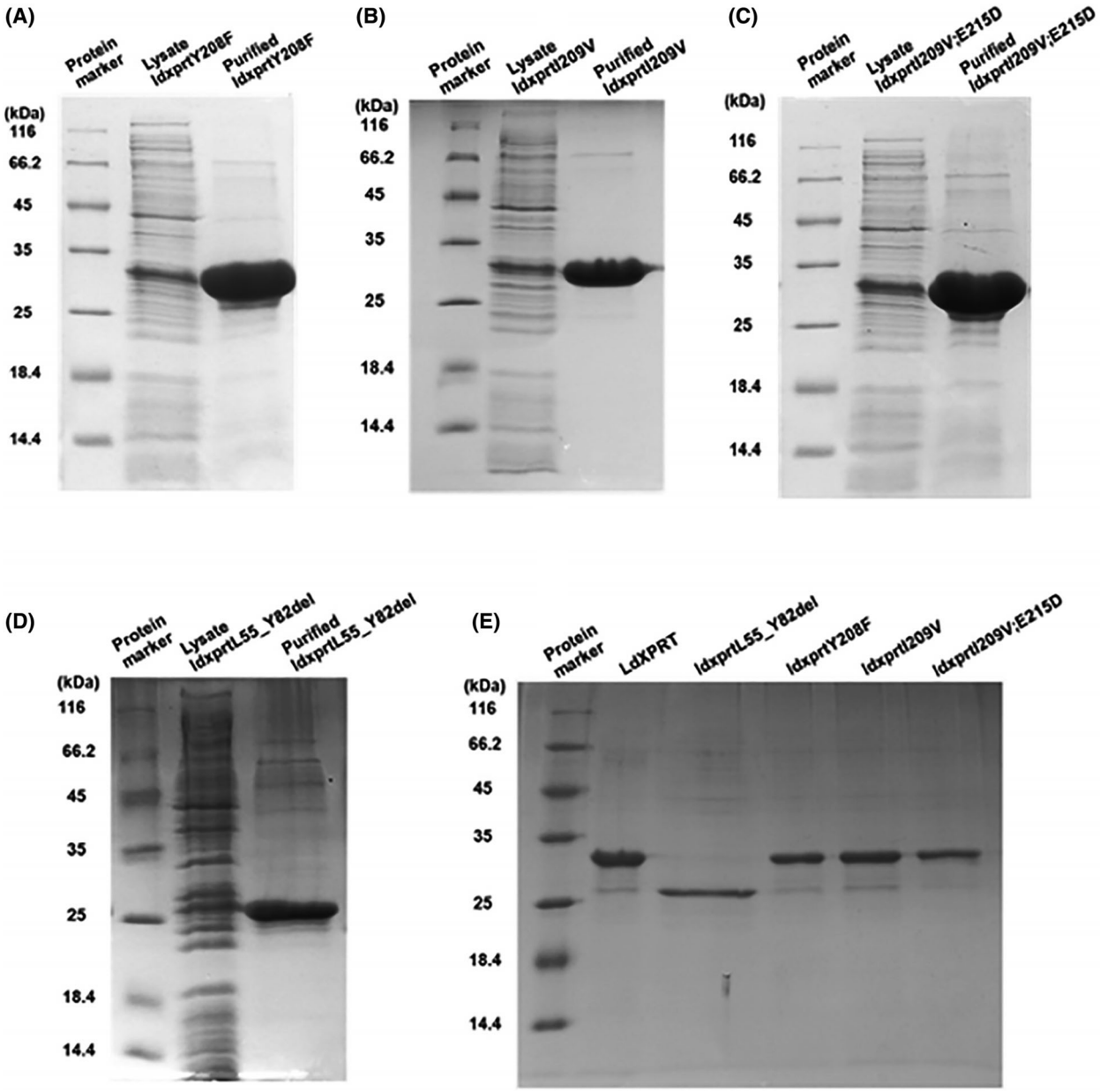

Fig. 3. SDS/PAGE analysis of the purified LdXPRT mutants. (A) ldxprtY208F; (B) ldxprtI209V; (C) ldxprtI209V;E215D; (D) ldxprtL55_Y82del; and (E) Comparison of LdXPRT with mutant proteins.

similar microenvironment surrounding the tyrosine residue. This is not the case in ldxprtI209V/E215D, since the position of glutamate which provides a carbonyl acceptor group to tyrosine for the conversion of tyrosinate is mutated to aspartate.

The binding affinities of mutants with XMP, IMP, and GMP were determined in terms of the dissociation constant (K_d), measured from the fluorescence quenching spectra. Fluorescence quenching was carried out by titrating the protein samples against ligands (Fig. 7). Wild-type enzyme showed K_d values of 5.16×10^{-5}, 10.28×10^{-5}, and 6.35×10^{-5} Mol for XMP, IMP, and GMP, respectively, indicating that it prefers XMP over IMP and GMP. The K_d values of ldxprtI209V and ldxprtI209V;E215D revealed that these two proteins have higher affinities for IMP and GMP than XMP (Table 1). LdxprtY208F showed a very minor shift in K_d of XMP and GMP with a notable decrease in K_d of IMP; however, its specificity remained the same as xanthine was a more favored

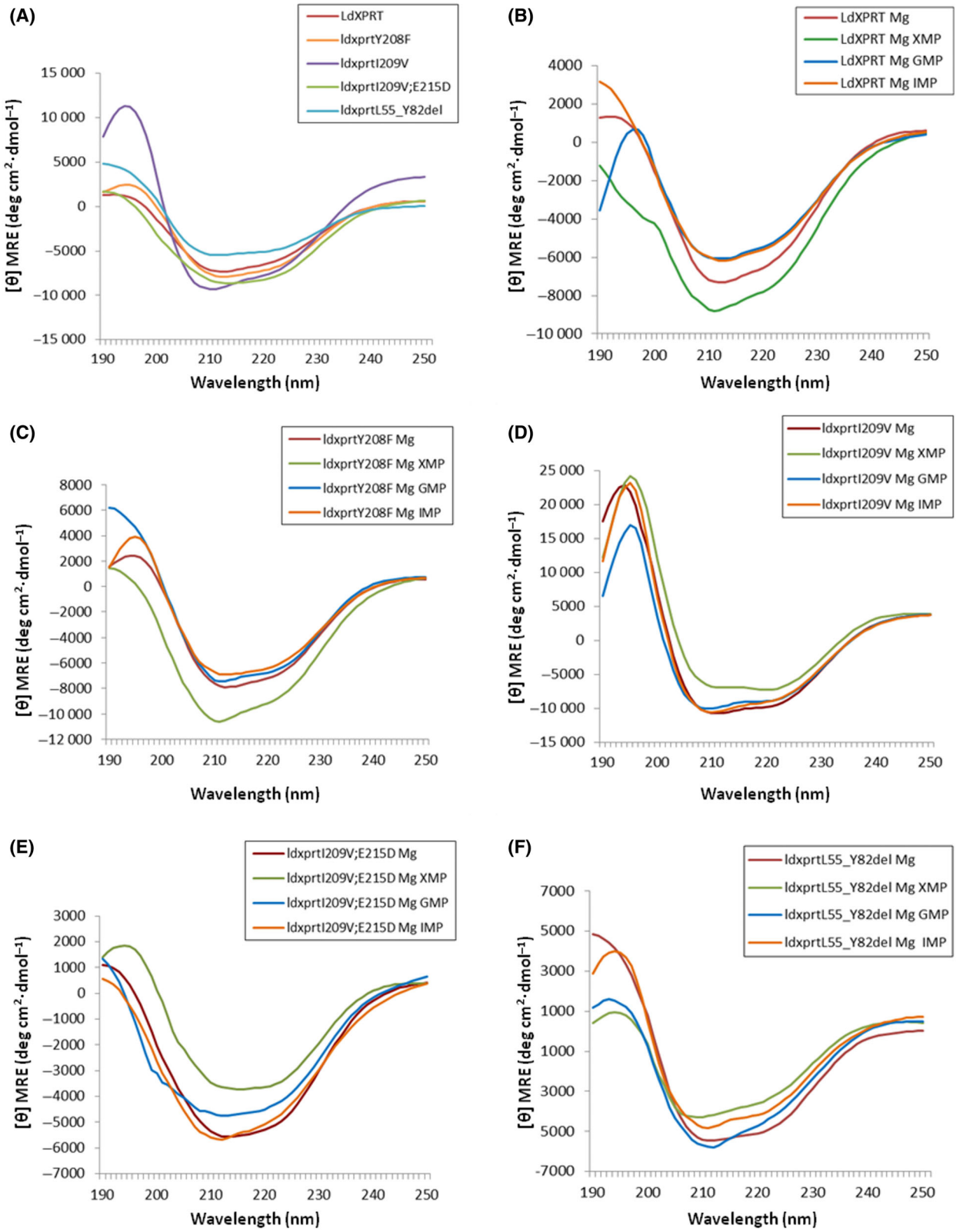

Fig. 4. Far-UV CD spectral analysis of LdXPRT mutants. (A) Far-UV CD spectra of wild-type LdXPRT and mutants; (B) LdXPRT with ligands; (C) ldxprtY208F with ligands; (D) ldxprtI209V with ligands; (E) ldxprtI209V;E215D with ligands; and (F) ldxprtL55_Y82del with ligands.

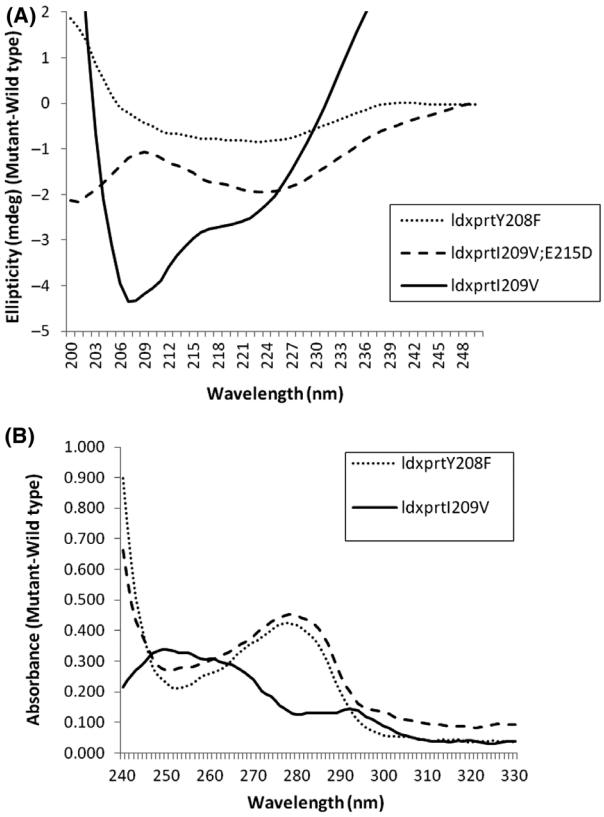

Fig. 5. Spectral analysis of LdXPRT mutants. (A) CD difference spectra were generated by subtracting the far-UV CD spectra of LdXPRT from the spectra of ldxprtY208F, ldxprtI209V, and ldxprtI209V;E215D. The spectra were recorded from 190 to 250 nm. (B) UV absorbance difference spectra were generated by subtracting the LdXPRT spectra from the spectra of ldxprtY208F, ldxprtI209V, and ldxprtI209V;E215D. The spectra were recorded from 240 to 330 nm.

substrate than hypoxanthine and guanine. The ldxprtL55_Y82del showed a significant increase in K_d for all three ligands indicating a decreased affinity for all.

Kinetic analysis of LdXPRT mutants

Kinetic analysis demonstrated that LdXPRT favors xanthine over hypoxanthine and guanine (Table 2). The K_m values of LdXPRT for xanthine, hypoxanthine, and guanine in Tris/HCl buffer, pH 7 were 8.9 ± 1.5, 204.2 ± 14.67, and 103.7 ± 15.24 μM, and the k_{cat} values were 1.8 ± 0.041, 1.1 ± 0.093, and 0.455 ± 0.042 s^{-1}, respectively. The ldxprtY208F showed a slight increase in K_m for xanthine (25.54 ± 2.9 μM) and a notable decrease in K_m values of hypoxanthine (82.21 ± 15.2 μM) and guanine (57.03 ± 17.87 μM). However, its specificity for nucleobases remains the same as that of LdXPRT (xanthine>guanine>hypoxanthine). The ldxprtI209V showed a

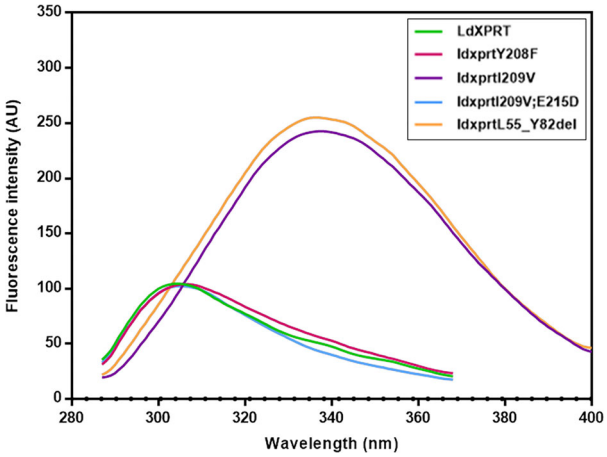

Fig. 6. Fluorescence emission spectra of mutants and wild-type LdXPRT.

sevenfold-eightfold increase in K_m for xanthine with a fourfold-eightfold decrease in K_m for hypoxanthine and twofold-sevenfold decrease in K_m for guanine. The K_m value of ldxprtI209V;E215D for xanthine was almost similar to that of ldxprtI209V with an additional decrease in K_m of hypoxanthine and guanine indicating that these mutations change the specificity of the enzyme for nucleobases. Surprisingly, ldxprtI209V;E215D showed a marked increase in k_{cat} values of all purine bases and PRPP; however, ldxprtI209V does not cause any significant change in k_{cat} values indicating that the Asp 215 is responsible for higher turnover rates. The ldxprtL55_Y82del did not show activity for any of the nucleobases suggesting the importance of this region in enzyme activity as the mutant protein in CD studies was found to be stable and in folded form.

Discussion

XPRT and HGPRT are the main enzymes for purine salvage in *L. donovani* and potential targets for designing antileishmanial agents [6,24]. LdXPRT is the focus of attention since long as it is absent from humans. The mutational studies of LdXPRT reported earlier were focused only on acidic residues of the purine-binding domain [11]. In the present study, we mutated all the differing active-site residues of LdXPRT from the purine-binding residues of HGPRT to identify the molecular determinants of its unique 6-oxopurine specificity. We also generated a mutant where the unique motif that was identified in leishmanial XPRT enzymes was deleted to elucidate its effect on the structure and activity of the enzyme. From sequence and structure comparison of LdXPRT with the crystal structure of *L. tarentolae* HGPRT, four purine-

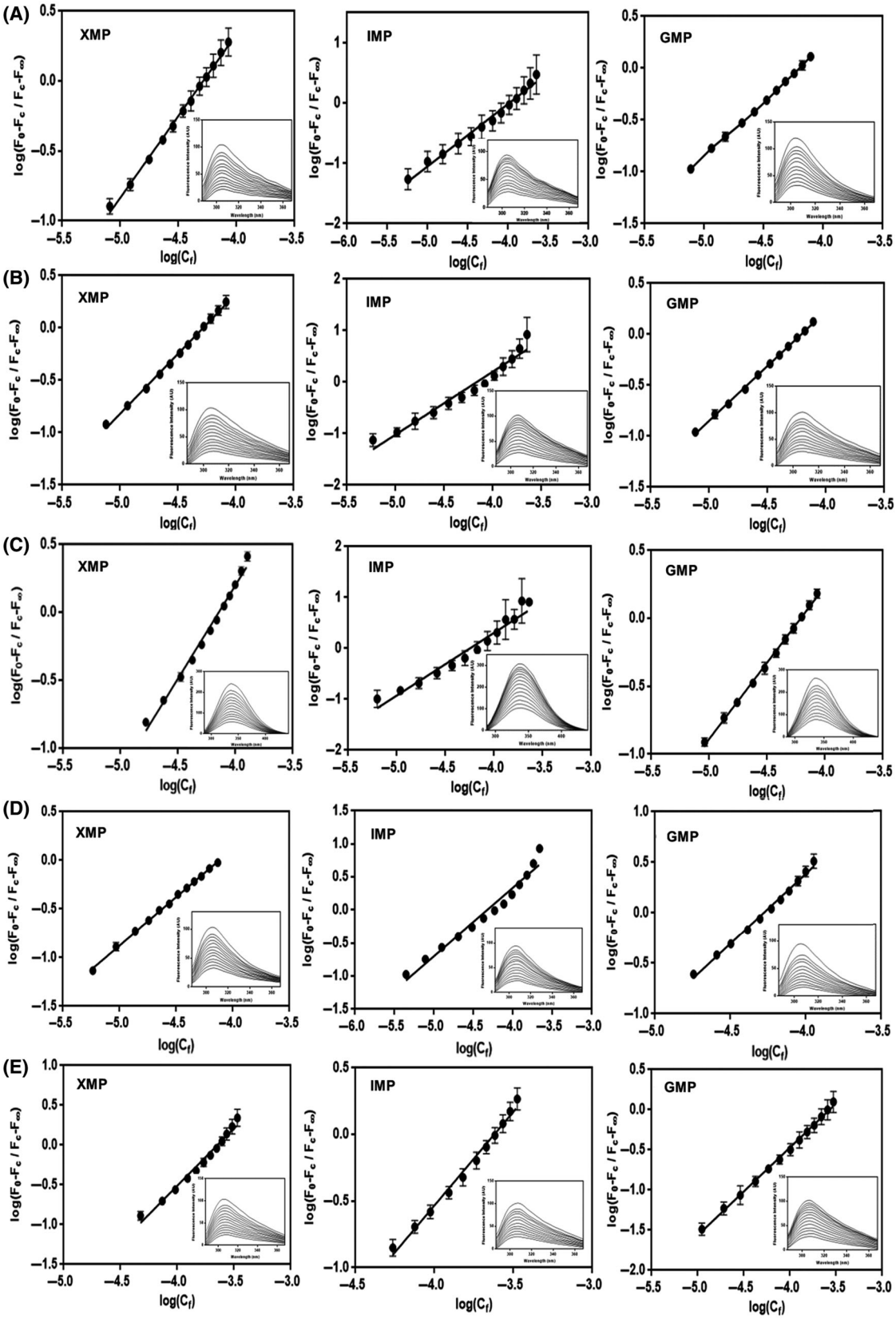

Fig. 7. Plots of fluorescence quenching for mutants and wild-type LdXPRT with ligands. The inset figures represent the progressive emission spectra of each enzyme upon addition of ligand. (A) LdXPRT; (B) ldxprtY208F; (C) ldxprtI209V; (D) ldxprtI209V;E215D; (E) ldxprtL55_Y82del. F0, Fc, and F∞ are the relative fluorescence emission intensity of the enzyme alone, the enzyme in the presence of a concentration (Cf) of ligand, and the intensity of enzyme saturated with ligand, respectively. Cf is the free ligand concentration in molarity. The dissociation constant (Kd) for each ligand was determined from the plot of log (Cf) versus log (F0-Fc/Fc-F∞) using antilog of X intercept when Y = 0, through the relation $K_d = 1/K_a$; where K_a = antilog (-pKa).

Table 1. Dissociation constants of mutant–ligand interactions determined by fluorescence spectroscopy.

Enzymes	XMP K_d (Mol)	IMP K_d (Mol)	GMP K_d (Mol)
LdXPRT	$5.16 \times 10^{-5} \pm 0.123$	$10.28 \times 10^{-5} \pm 0.402$	$6.35 \times 10^{-5} \pm 0.167$
ldxprtY208F	$5.19 \times 10^{-5} \pm 0.063$	$6.8 \times 10^{-5} \pm 1.220$	$6.13 \times 10^{-5} \pm 0.016$
ldxprtI209V	$7.21 \times 10^{-5} \pm 1.040$	$5.63 \times 10^{-5} \pm 0.830$	$6.16 \times 10^{-5} \pm 0.085$
ldxprtI209V;E215D	$7.58 \times 10^{-5} \pm 0.824$	$4.7 \times 10^{-5} \pm 0.391$	$5.24 \times 10^{-5} \pm 0.454$
ldxprtL55_Y82del	$22.59 \times 10^{-5} \pm 2.13$	$26.85 \times 10^{-5} \pm 1.55$	$23.87 \times 10^{-5} \pm 1.45$

binding residues (Lys 186, Tyr 208, Ile 209, and Glu 215) were identified in the binding site of LdXPRT. The Lysine residue (Lys 186) was conserved in all PRTs whereas Tyr 208, Ile 209, and Glu 215 were replaced by Phe, Val, and Asp, respectively, in most of the HGPRT enzymes (Fig. 2 & Table 3).

The substitution of Tyr 208 by Phe did not cause any significant change in the purine base specificity of the LdXPRT. A previous report on mutation study of *T. foetus* HGXPRT [9] also showed that Y156W and Y156F do not cause any significant change in the nucleobase specificity of the enzyme, hence suggesting that the interactions of the hydroxyl group of Tyr 208 with the exocyclic C-2 substituent of the purine ring might be minimal and the interactions between aromatic amino acids and the purine ring might be limited to the pi-pi binding forces. The ldxprtI209V and ldxprtI209V;E215D showed a significant decrease in affinity for xanthine and increased affinity for hypoxanthine and guanine. Similar substrate specificities were also observed in most of the PRTs (Table 3) having Val at the corresponding position; they show negligible or no activity for xanthine. The *G. lamblia* GPRT [25] also has Val at the corresponding position, and it also does not have specificity for xanthine. Enzymes having Gln (*B. subtilis* [26] and *S. faecalis* XPRT [27]) in place of Ile 209 of LdXPRT have a strong affinity for xanthine but a negligible affinity for hypoxanthine and guanine whereas those PRTs (*T. gondi* and *T. foetus* HGXPRT, LdXPRT) having Ile in this position can recognize all three purine bases (Table 3). Hence, it suggests that the Ile 209 in LdXPRT might be responsible for the affinity of LdXPRT for all three purine bases with good affinity toward xanthine whereas Val at the corresponding position might reduce the affinity for xanthine. The only exception in this pattern is the *T. brucei* HGXPRT (Table 3) which despite having Val at this position showed a higher affinity for xanthine. The authors have speculated that this may be due to the formation of the hydrogen bond between the hydroxyl group of Tyr 201 and the main-chain carbonyl oxygen of Glu 208 which assisted the binding of xanthine/XMP by holding the base in place [28].

Previous mutational studies of E215D [11] and D163E [9] in LdXPRT and *T. foetus* HGXPRT, suggested that these single point mutations do not give any significant change in the purine base specificity of the enzyme. However, in the present study the double mutant ldxprtI209V;E215D showed a ~ twofold-threefold decrease in K_m for hypoxanthine and guanine without alteration in the K_m of xanthine compared to ldxprtI209V (Table 2). Hence, the I209V and I209V;E215D mutations converted LdXPRT to a HGXPRT-like enzyme which exhibits nucleobase specificity comparable to *T. gondi* [8], *T. foetus* [9], and *P. falciparum* [29] HGXPRTs. Surprisingly, ldxprtI209V;E215D gives a marked increase in turnover rates with all purine bases. Such increased catalytic efficiency was also observed in the single mutant E215D [11] indicating that the presence of Asp might be responsible for the increased turnover rates of the enzyme. In many HGPRTs, this Asp in addition to direct interactions with the purine ring is also involved in binding to an Mg atom that is linked through a water molecule to the purine substrate and helps to orient the purine base for catalysis [30–32].

CD spectroscopic studies revealed that the ldxprtI209V causes alteration in the phenylalanine side chains of the protein whereas the ldxprtY208F and the ldxprtI209V;E215D cause an alteration in the local environment of the tyrosine residues. CD analysis also suggested that the binding of XMP to ldxprtI209V,

Table 2. Kinetic parameters of enzyme assay for mutants and wild-type LdXPRT. NA represents no enzyme activity.

Enzymes	Xanthine			Hypoxanthine			Guanine			PRPP (Xanthine)			PRPP (Hypoxanthine)		
	K_m (μM)	k_{cat} (s^{-1})	k_{cat}/K_m (s^{-1} μM^{-1})	K_m (μM)	k_{cat} (s^{-1})	k_{cat}/K_m (s^{-1} μM^{-1})	K_m (μM)	k_{cat} (s^{-1})	k_{cat}/K_m (s^{-1} μM^{-1})	K_m (μM)	k_{cat} (s^{-1})	k_{cat}/K_m (s^{-1} μM^{-1})	K_m (μM)	k_{cat} (s^{-1})	k_{cat}/K_m (s^{-1} μM^{-1}) $^{-1}$
LdXPRT	8.9 ± 1.5	1.8 ± 0.041	0.2022	204.2 ± 54.67	1.1 ± 0.093	0.0053	103.7 ± 15.24	0.455 ± 0.042	0.0043	18.85 ± 4.5	2 ± 0.054	0.106	41.76 ± 12.41	1.3 ± 0.056	0.0311
ldxprty208f	25.54 ± 2.9	1.126 ± 0.029	0.044	82.21 ± 15.2	0.577 ± 0.04	0.0070	57.03 ± 17.87	0.308 ± 0.03	0.0054	19.54 ± 6.4	0.81 ± 0.03	0.0414	32.53 ± 9.1	1.1 ± 0.036	0.0338
ldxprti209v	66.62 ± 8.3	4.19 ± 0.18	0.0628	48.62 ± 14.27	1.23 ± 0.067	0.0252	37.30 ± 4.16	0.518 ± 0.016	0.0138	29.9 ± 4.75	4.38 ± 0.09	0.146	35.76 ± 6.84	1.21 ± 0.029	0.0338
ldxprti209v;E215D	60.98 ± 6.73	15.92 ± 0.59	0.2610	26.49 ± 8.83	9.89 ± 0.41	0.3733	14.41 ± 2.52	8.68 ± 0.24	0.6023	36.69 ± 7.06	13.29 ± 0.36	0.3622	22.57 ± 4.67	7.99 ± 0.27	0.3540
ldxprt-L55_Y82-del	NA	NA	NA	NA	NA	NA	NA	NA	NA	NA	NA	NA	NA	NA	NA

ldxprtI209V;E215D, and ldxprtL55_Y82del requires higher structural change than the IMP and GMP (Fig. 4D–F). It was also observed that the binding of GMP to the proteins having Ile 209 (LdXPRT, ldxprtY208F, and ldxprtL55_Y82del) in the purine-binding pocket causes the alteration in the environments of aromatic side chains of the proteins.

In our previous report, we identified a unique motif (Leu 55 to Tyr 82) in the LdXPRT sequence which was absent in most of the PRTs including leishmanial, human, and trypanosomal HGPRTs. The region was predicted to be involved in stabilizing the interaction of the enzyme with the substrate during the enzyme reaction [4]. The deletion of this region from the enzyme caused the increase in K_d (Table 1) for all the three nucleotides and loss of activity in enzyme assay (Table 2) indicating its importance in enzyme activity since the protein was stable and in folded form.

LdXPRT is a protein with the remarkable ability to recognize more than one substrate albeit with different catalytic efficiencies. Our biochemical investigations with the mutants of LdXPRT have unraveled key residues that allow LdXPRT to act as an XPRT and not as an HGXPRT. A single residue mutation of isoleucine that interacts with the C-2 substituent group of the purine ring to a valine could modulate LdXPRT specificity for binding to xanthine and make it behave more like an HGXPRT. Understanding the active-site residues which determine the structural discrimination of different purine substrates will be helpful to design specific inhibitors against this potential antileishmanial drug target. The present study can be further enhanced by crystal structures of LdXPRT and its mutants with different substrates which can throw more light on how precisely these binding site residues assemble in order to achieve nucleobase specificity.

Acknowledgements

This work was primarily funded by Science & Engineering Research Board [grant number SR/FT/LS-56/2010], Department of Biotechnology [grant number BT/BI/O4/070/2006], and Indian Council of Medical Research [grant number 80/928/2015-ECD-1] and [6/9-7(230)/2020-ECD-II], Government of India. We express our thanks to IIT Gandhinagar and Nirma University for providing CD and Fluorescence facilities, respectively. We thank Puri Foundation for Education in India for all infrastructural support and financial assistance. We thank Dr. Reena A Rajput, University of IAR for technical and administrative support. We acknowledge Prof. Jayanta Kumar Pal, Savitribai

Table 3. List of 6-oxopurine PRTs showing their active-site residues and K_m values for nucleobase substrates. The active-site residues were determined from multiple sequence alignment and structure superposition (https://www.rcsb.org/). NA represents No activity.

Active site residues	Source organisms	Enzymes	K_m (μm)			References
			Xanthine	Hypoxanthine	Guanine	
Y_I_E	*L. donovani*	XPRT	7.1	204	103	Present study
F_Q_L	*B. subtilis*	XPRT	2.2	1250	281	[26]
F_Q_L	*S. faecalis*	XPRT	20	-	NA	[27]
T_W_D	*E. coli*	XGPRT	30.5	90.8	4.3	[33]
W_I_D	*T. gondi*	HGXPRT	14.4	1.6	2.1	[8]
Y_I_D	*T. foetus*	HGXPRT	6.1	3	2.4	[9]
F_V_D	*P. falciparam*	HGXPRT	420	0.9	1.4	[7]
Y_V_E	*T. brucei*	HGXPRT	2.8	17.3	13.0	[13]
F_V_D	*T. brucei*	HGPRT	221	5.5	2.3	[28]
F_V_D	*T. cruzi*	HGPRT	NA	8.63	12.4	[34]
F_V_D	*L. donovani*	HGPRT	NA	6.1	5	[35]
F_V_D	*L. tarentolae*	HGPRT	NA	4.4	2.8	[36]
F_V_D	*H. sapiens*	HGPRT	NA	1.4	4.5	[37]
F_V_D	*T. tengcongensis*	HGPRT	> 200	2.4	3.6	[38]
F_V_D	*S. mansoni*	HGPRT	NA	3.7	2.1	[39]
F_V_D	*M. tuberculosis*	HGPRT	NA	26	10	[40]
Y_V_D	*T. thermophilous*	HGPRT	NA	3.9	7.4	[41]
Y_V_E	G. lamblia	GPRT	NA	> 200	16.4	[25]

Phule Pune University, India, and Prof. Vikash Kumar Dubey, IIT (BHU), India, for providing *L. donovani* genomic DNA and Ms. Nidhi Darji for technical assistance.

Data accessibility

Research data pertaining to this article are located at figshare.com.

The data that support the findings of this study are available from the corresponding author [anju.p@cu-g.ac.in] upon reasonable request.

References

1 Berens RL, Krug EC and Marr JJ (1995) Purine and Pyrimidine Metabolism. In Biochemistry and Molecular Biology of Parasites (Marr JJ and Müller M, eds), pp. 89–117. Academic Press, Cambridge, MA.

2 Boitz JM, Ullman B, Jardim A and Carter NS (2012) Purine salvage in Leishmania: complex or simple by design? *Trends Parasitol* **28**, 345–352.

3 Boitz JM and Ullman B (2006) A conditional mutant deficient in hypoxanthine-guanine phosphoribosyltransferase and xanthine phosphoribosyltransferase validates the purine salvage pathway of Leishmania donovani. *J Biol Chem* **281**, 16084–16089.

4 Patel B, Patel D, Parmar K, Chauhan R, Singh DD and Pappachan A (2018) L. donovani XPRT: molecular characterization and evaluation of inhibitors. *Biochim Biophys Acta* **1866**, 426–441.

5 Boitz JM and Ullman B (2006) Leishmania donovani singly deficient in HGPRT, APRT or XPRT are viable in vitro and within mammalian macrophages. *Mol Biochem Parasitol* **148**, 24–30.

6 Jardim A, Bergeson SE, Shih S, Carter N, Lucas RW, Merlin G, Myler PJ, Stuart K and Ullman B (1999) Xanthine phosphoribosyltransferase from Leishmania donovani. Molecular cloning, biochemical characterization, and genetic analysis. *J Biol Chem* **274**, 34403–34410.

7 Keough D, Ng A-L, Winzor D, Emmerson B and de Jersey J (1999) Purification and characterization of Plasmodium falciparum hypoxanthine–guanine–xanthine phosphoribosyltransferase and comparison with the human enzyme. *Mol Biochem Parasitol* **98**, 29–41.

8 Heroux A, White EL, Ross LJ, Davis RL and Borhani DW (1999) Crystal structure of Toxoplasma gondii hypoxanthine-guanine phosphoribosyltransferase with XMP, pyrophosphate, and two Mg(2+) ions bound: insights into the catalytic mechanism. *Biochemistry* **38**, 14495–14506.

9 Munagala NR and Wang CC (1998) Altering the purine specifcity of hypoxanthine-guanine-xanthine phosphoribosyltransferase from tritrichomonas foetus by structure-based point mutations in the enzyme protein. *Biochemistry* **37**, 16612–16619.

10 Lee CC, Craig SP and Eakin AE (1998) A single amino acid substitution in the human and a bacterial hypoxanthine phosphoribosyltransferase modulates

specificity for the binding of guanine. *Biochemistry* **37**, 3491–3498.
11 Ullman B, Cyr N, Choi K and Jardim A (2010) Acidic residues in the purine binding site govern the 6-oxopurine specificity of the Leishmania donovani xanthine phosphoribosyltransferase. *Int J Biochem Cell Biol* **42**, 253–262.
12 Waterhouse A, Bertoni M, Bienert S, Studer G, Tauriello G, Gumienny R, Heer FT, de Beer TAP, Rempfer C, Bordoli L *et al.* (2018) SWISS-MODEL: homology modelling of protein structures and complexes. *Nucleic Acids Res* **46**, W296–W303.
13 Terán D, Doleželová E, Keough DT, Hocková D, Zíková A and Guddat LW (2019) Crystal structures of Trypanosoma brucei hypoxanthine – guanine – xanthine phosphoribosyltransferase in complex with IMP, GMP and XMP. *FEBS J* **286**, 4721–4736.
14 Xu D and Zhang Y (2011) Improving the physical realism and structural accuracy of protein models by a two-step atomic-level energy minimization. *Biophys J* **101**, 2525–2534.
15 Lovell SC, Davis IW, Arendall WB, De Bakker PIW, Word JM, Prisant MG, Richardson JS and Richardson DC (2003) Structure validation by Cα geometry: φ, ψ and Cβ deviation. *Proteins Struct Funct Genet* **50**, 437–450.
16 Luthy R, Bowie JU and Eisenberg D (1992) Assessment of protein models with three-dimensional profiles. *Nature* **356**, 83–85.
17 Colovos C and Yeates TO (1993) Verification of protein structures: patterns of nonbonded atomic interactions. *Protein Sci* **2**, 1511–1519.
18 Schrodinger LLC (2015) The PyMOL molecular graphics system. Version 1.8.
19 Larkin MA, Blackshields G, Brown NP, Chenna R, McGettigan PA, McWilliam H, Valentin F, Wallace IM, Wilm A, Lopez R *et al.* (2007) Clustal W and Clustal X version 2.0. *Bioinformatics* **23**, 2947–2948.
20 Laemmli UK (1970) Cleavage of structural proteins during the assembly of the head of bacteriophage T4. *Nature* **227**, 680–685.
21 Freifelder D (1976) Physical biochemistry: Applications to biochemistry and molecular biology. San Francisco: W.H. Freeman and Company.
22 Vuilleumier S, Sancho J, Loewenthal R and Fersht AR (1993) Circular dichroism studies of barnase and its mutants: characterization of the contribution of aromatic side chains. *Biochemistry* **32**, 10303–10313.
23 Jordano J, Barbero JL, Montero F and Franco L (1983) Fluorescence of histones H1. A tyrosinate-like fluorescence emission in Ceratitis capitata H1 at neutral pH values. *J Biol Chem* **258**, 315–320.
24 Parihar PS and Pratap JV (2020) The L.donovani Hypoxanthine-guanine phosphoribosyl transferase (HGPRT) oligomer is distinct from the human homolog. *Biochem Biophys Res Commun* **532**, 499–504.
25 Page JP, Munagala NR and Wang CC (1999) Point mutations in the guanine phosphoribosyltransferase from Giardia lamblia modulate pyrophosphate binding and enzyme catalysis. *Eur J Biochem* **259**, 565–571.
26 Arent S, Kadziola A, Larsen S, Neuhard J and Jensen KF (2006) The Extraordinary specificity of xanthine phosphoribosyltransferase from bacillus subtilis elucidated by reaction kinetics, ligand binding, and crystallography. *Biochemistry* **45**, 6615–6627.
27 Miller RL, Adamczyk DL, Fyfe JA and Elion GB (1974) Xanthine phosphoribosyltransferase from Streptococcus faecalis: Properties and specificity. *Arch Biochem Biophys* **165**, 349–358.
28 Terán D, Hocková D, Česnek M, Zíková A, Naesens L, Keough DT and Guddat LW (2016) Crystal structures and inhibition of Trypanosoma brucei hypoxanthine-guanine phosphoribosyltransferase. *Sci Rep* **6**, 35894.
29 Roy S, Nagappa LK, Prahladarao VS and Balaram H (2015) Kinetic mechanism of Plasmodium falciparum hypoxanthine-guanine-xanthine phosphoribosyltransferase. *Mol Biochem Parasitol* **204**, 111–120.
30 Focia PJ, Craig SP 3rd, Nieves-Alicea R, Fletterick RJ and Eakin AE (1998) A 1.4 A crystal structure for the hypoxanthine phosphoribosyltransferase of Trypanosoma cruzi. *Biochemistry* **37**, 15066–15075.
31 Heroux A, White EL, Ross LJ, Kuzin AP and Borhani DW (2000) Substrate deformation in a hypoxanthine-guanine phosphoribosyltransferase ternary complex: the structural basis for catalysis. *Structure* **8**, 1309–1318.
32 Shi W, Munagala NR, Wang CC, Li CM, Tyler PC, Furneaux RH, Grubmeyer C, Schramm VL and Almo SC (2000) Crystal structures of Giardia lamblia guanine phosphoribosyltransferase at 1.75 A. *Biochemistry* **39**, 6781–6790.
33 Vos S, de Jersey J and Martin JL (1997) Crystal structure of escherichia coli xanthine phosphoribosyltransferase. *Biochemistry* **36**, 4125–4134.
34 Wenck MA, Medrano FJ, Eakin AE and Craig SP (2004) Steady-state kinetics of the hypoxanthine phosphoribosyltransferase from Trypanosoma cruzi. *Biochim Biophys Acta* **1700**, 11–18.
35 Jardim A and Ullman B (1997) The conserved serine-tyrosine dipeptide in Leishmania donovani hypoxanthine-guanine phosphoribosyltransferase is essential for catalytic activity. *J Biol Chem* **272**, 8967–8973.
36 Monzani PS, Alfonzo JD, Simpson L, Oliva G and Thiemann OH (2002) Cloning, characterization and preliminary crystallographic analysis of Leishmania hypoxanthine–guanine phosphoribosyltransferase. *Biochim Biophys Acta* **1598**, 3–9.

37 Raman J, Sumathy K, Anand RP and Balaram H (2004) A non-active site mutation in human hypoxanthine guanine phosphoribosyltransferase expands substrate specificity. *Arch Biochem Biophys* **427**, 116–122.
38 Chen Q, You D, Hu M, Gu X, Luo M and Lu S (2003) Cloning, purification, and characterization of thermostable hypoxanthine–guanine phosphoribosyltransferase from Thermoanaerobacter tengcongensis. *Protein Expr Purif* **32**, 239–245.
39 Yuan L, Craig SP, McKerrow JH and Wang CC (1990) The hypoxanthine-guanine phosphoribosyltransferase of Schistosoma mansoni. Further characterization and gene expression in Escherichia coli. *J Biol Chem* **265**, 13528–13532.
40 Patta PC, Martinelli LKB, Rotta M, Abbadi BL, Santos DS and Basso LA (2015) Mode of action of recombinant hypoxanthine–guanine phosphoribosyltransferase from Mycobacterium tuberculosis. *RSC Adv* **5**, 74671–74683.
41 Kanagawa M, Baba S, Ebihara A, Shinkai A, Hirotsu K, Mega R, Kim K, Kuramitsu S, Sampei G and Kawai G (2010) Structures of hypoxanthine-guanine phosphoribosyltransferase (TTHA0220) from Thermus thermophilus HB8. *Acta Crystallogr Sect F Struct Biol Cryst Commun* **66**, 893–898.

Supporting information

Additional supporting information may be found online in the Supporting Information section at the end of the article.

Fig S1. Near-UV CD spectral analysis of LdXPRT mutants with ligands.

Table S1. The list of oligos for the PCR amplification of LdXPRT mutants.

Table S2. Ramachandran plot, Verify 3D, and ERRAT plot scores of LdXPRT model before and after energy minimization.